



Scholars Research Library

Archives of Physics Research, 2018, 9(1): 17-25
(<http://scholarsresearchlibrary.com/archive.html>)



ISSN 0976-0970
CODEN (USA): APRRC7

Growth and Studies on Succinic Acid Doped Zinc Sulphate Single Crystals

T Lidia Arockia Thai^{1*}, S Mary Delphine²

¹College of Engineering and Petroleum, Kuwait University, Kuwait

²Holy Cross College, Nagercoil, India

*Corresponding Author: T Lidia Arockia Thai, College of Engineering and Petroleum, Kuwait University, Kuwait
India, E-mail: lidiasekar@gmail.com

ABSTRACT

Single crystals of pure and succinic acid doped zinc sulphate heptahydrate crystals were grown by slow evaporation technique. The grown crystals of pure and succinic acid doped zinc sulphate heptahydrate were analyzed using FTIR to estimate qualitatively the presence of the functional groups. The thermal stability of the grown crystals was studied by using TG/DTA analysis. Dielectric studies were carried out on the grown crystals at three different temperatures.

Keywords: Succinic acid, Zinc sulphate heptahydrate, FTIR, Dielectric constant, Differential thermal analysis and Thermogravimetry

INTRODUCTION

Metal-organic coordination compounds have been of extensive importance due to their wide range of applications in opto electronics such as integrated optics, optical switching, telecommunications, bistability and modulation [1,2]. Although organic materials exhibit excellent nonlinear optical properties they get damaged during processing due to poor thermal and mechanical properties [3-7]. The metal-organic materials have the potential to combine the high optical nonlinearity and chemical flexibility of organics with the physical properties of inorganics. The process of adding organic additives accelerates the growth rate of crystals and can be used to grow large size crystals with better transparency and mechanical properties compared to the pure counterparts [8,9]. In the present investigation we have grown crystals by adding 0.01, 0.03, 0.05, 0.07 and 0.09 mol% of succinic acid (SA) to zinc sulphate heptahydrate (ZSH). Hence defect free crystals of succinic acid doped zinc sulphate heptahydrate (ZSHSA) crystals for five different molar concentrations were grown by slow evaporation technique and are compared with the pure, defect free and fully grown ZSH crystals. The grown crystals were subjected to PXRD, TG/DTA analysis, FTIR spectroscopic analysis and dielectric studies.

EXPERIMENTAL

The flawless crystals of ZSHSA were grown by dissolving high purity $\text{ZnSO}_4 \cdot 7\text{H}_2\text{O}$ and $(\text{CH}_2\text{COOH})_2$ from Sigma Aldrich, in deionized double distilled water. Optically transparent ZSHSA crystals were grown by slow evaporation method in a period of three weeks from the mother solutions which were prepared in the appropriate proportions of 1:0.01, 1:0.03, 1:0.05, 1:0.07 and 1:0.09 mole concentrations of ZSH:SA respectively, while for ZSH crystals the solution was prepared by dissolving high purity $\text{ZnSO}_4 \cdot 7\text{H}_2\text{O}$ in deionized double distilled water. X-ray diffraction analysis of the grown crystals was carried out using RICH, SEIFERT, XRD 3000 P with $\text{CuK}\alpha$ ($\lambda=0.15406$ nm). Qualitative analysis of the presence of functional groups in the grown crystals were recorded by Perkin Elmer Fourier Transform infrared spectrometer (Model: Spectrum RXI) using KBr pellet method in the range of $400\text{--}4000$ cm^{-1} . The thermal behavior of the ZSHSA and ZSH crystals were characterized using thermo gravimetric analysis (TGA) and differential thermal analysis (DTA) by SDTQ 600 V 8.2 thermal analyzer in the temperature range $10\text{--}1000^\circ\text{C}$. The dielectric studies of the grown crystals were carried out using LCR meter (Agilent 4284).

RESULTS AND DISCUSSION

Powder X-ray diffraction analysis

The powder X-ray diffraction (PXRD) spectra of the ZSH and ZSHSA are shown in the Figure 1. The sharp peaks depict the crystalline nature of the grown crystals. The lattice parameters of the unit cell of the grown ZSH and the doped ZSHSA crystals, tabulated in Table 1, were found to be in good agreement with the ZSH unit cell parameters reported by Krishna Priya et al [10]. All of these crystals are found to be orthorhombic and belong to the $P2_12_12_1$ space group [11].

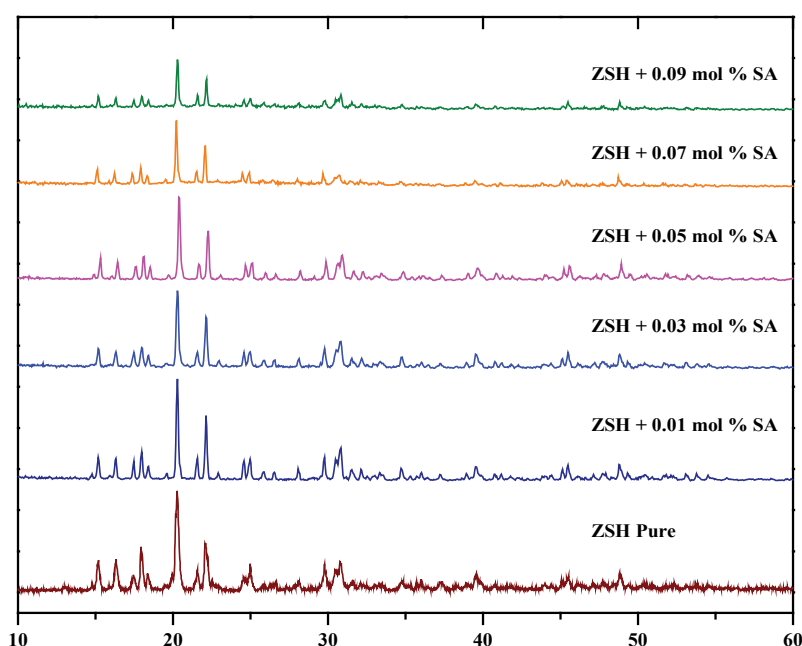


Figure 1: XRD spectra of ZSH and ZSHSA crystals

Crystal Data	Pure ZSH	ZSH+0.01 mol% SA	ZSH+0.03 mol% SA	ZSH+0.05 mol% SA	ZSH+0.07 mol% SA	ZSH+0.09 mol% SA
a (in Å)	12.83865	12.78814	12.7807	12.75315	12.79478	12.77966
b (in Å)	11.98457	12.02043	12.01595	11.91562	12.08422	12.01428
c (in Å)	5.73798	5.71455	5.71631	5.67498	5.73884	5.70752

Table 1: Unit cell parameters of ZSH and ZSHSA crystals

FTIR analysis

The FT-IR spectroscopy technique is a diverse and versatile analytical technique used to identify the functional groups present in the molecule based on the vibrational spectrum of the molecule and hence used in material characterization. It can be used for both organic and inorganic compounds. The frequency assignments of the absorption peaks for ZSH and the five

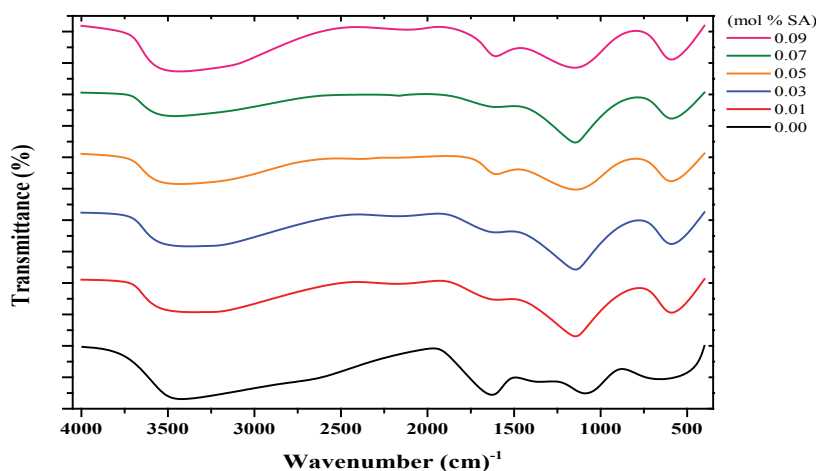


Figure 2: FTIR Transmission Spectra of ZSH and ZSHSA crystals

ZSHSA grown crystals are listed in the Table 2. The occurrence of the absorption in the range of 1750-1700 cm^{-1} , is found to be in the lower end of the range, roughly close to 1700 cm^{-1} , which confirms the presence of carboxylic acid salt and its conjugation with another carbonyl group, as the absorption peaks are not present in the middle of the range mentioned above. Hence it confirms the presence of two carboxylic groups, which can be interpreted as the presence of succinate in the ZSHSA crystals. The absence of absorption in the range of 1420-1370 cm^{-1} or 1200-1180 cm^{-1} [12], indicates the absence of organic sulphates in the ZSHSA crystals. Typically, this absorption, that is intense and broad in the range of 1130-1080 cm^{-1} [12], shows the presence of sulfate ion which is also consolidated by another absorption that has weak to medium intensity in the range of 680-610 cm^{-1} [12]. The occurrence of an absorption in the range of 1560-1520 cm^{-1} [17], is due to the asymmetric stretch of RCOO^- which is absent for that of an acid – RCOOH and hence it can be perceived as an additional confirmation of succinate in the ZSHSA crystal lattice. The transmission spectra of the ZSH and the five differently doped ZSHSA crystals are shown in the Figure 2.

Table 2: Fundamental frequencies of vibrations of ZSH and ZSHSA crystals

ZSH	Concentration of SA added to 1 mol % of ZSH					Functional group assignments
	0.01 mol%	0.03 mol%	0.05 mol%	0.07 mol%	0.09 mol%	
3522.81	3492.60	3489.17	3503.54	3555.26	3552.26	H bonded O–H, adsorbed water H–O–H stretching [13,14]
-	3232	3236	-	3240	3261	Succinic (Carboxylic) acid [15]
-	2159.87	2161.74	2162.36	2160.79	2160.36	CO adsorbed on zinc ions [16]
-	2089.48	2088.41	2088.66	2092.87	2085.68	Zinc (transition metal) carbonyls [12]
-	1709	1716	1719	1718	-	Zinc associated carbonyl groups [17]; Succinic (Carboxylic) acid derivatives [15]
1652.91	1614.06	1616.28	1615.53	1614.69	1616.62	H–O–H bending of water [14]
-	1512.69	1520.82	-	1521	1521.00	Succinic acid salt (Carboxylate) [12,17]
1121.70	1152.98	1153.49	1150.42	1152.85	1151.93	S=O Sulfates [12,18,19]
	1101.10	1100.74	1101.10	1102.10	1104.36	
860.16	865.83	865.64	864.84	865.91	863.92	H bonded O–H out-of-plane bending [12]
677.80,	652,	611.90	613.06	649,	612.62	Sulphate [12,19]
633.036	610.57			610.58		

Thermal characterization

The weight loss and the thermal stability of the grown ZSHSA crystals were studied by SDT Q600 V8.2 thermal analyzer. The ZSHSA crystals were crushed to a fine powder and subjected to a temperature range of 30-800°C, at a rate of 15°C/min, in an inert nitrogen atmosphere to perform the TGA and DTA analyses. The TG/DTA curves for two

doping concentrations of the ZSHSA crystals namely, 0.01 and 0.09 mol% SA are shown in the Figure 3, to compare and contrast. Both, the former sample of initial weight 5.617 mg and the latter of 5.668 mg, were thermally stable up to 43.66-44.38°C. The first weight loss occurred with sharp endothermic deep peaks in the DTA curve at 77.24°C and 79.15°C, respectively, as the former lost five molecules of water and the latter lost five and half a molecules of water. This accounted for a major weight loss of 31.51% and 31.83%, respectively, in the entire thermal process. The compounds started their second weight loss at 223.07°C and 223.58°C, resulting in the weight loss of 7.96% and 8.41%, respectively, due to loss of one and half a molecule of water, in the lattice site [20], summing up to loss of 7 water molecules for the latter and 6½ for the former. These weight losses might be due to the expulsion of the physically adsorbed water molecules [21,22]. The endothermic dips corresponding to these weight losses noticed in the DTA curves at 258.99°C and 260.93°C are assigned to the melting point of the crystal [23]. From Figure 3, we can notice a small exothermic peak in the DTA curve at 275.11°C for the former, while it is absent in the latter, which might be due to the liberation of volatile substances [24]. From 291.57°C and 293.31°C, respectively, the samples remained fairly stable that was inferred from the plateau of the TG curve until the next weight loss took place at the onset of 644.25°C and 638.61°C, respectively, with the loss of a carbon monoxide molecule observed with a 10.09% and 10.99% of weight loss substantiated by the endothermic decomposition peaks in the DTA curve at 758.73°C and 757.44°C, respectively, correspond to the melting point of the residue [23]. The left out materials may be the mixtures of the ZnO and carbon, based on the calculation of the loss of weight [25]. It was found that there was a very good agreement between the calculated and experimental weight loss.

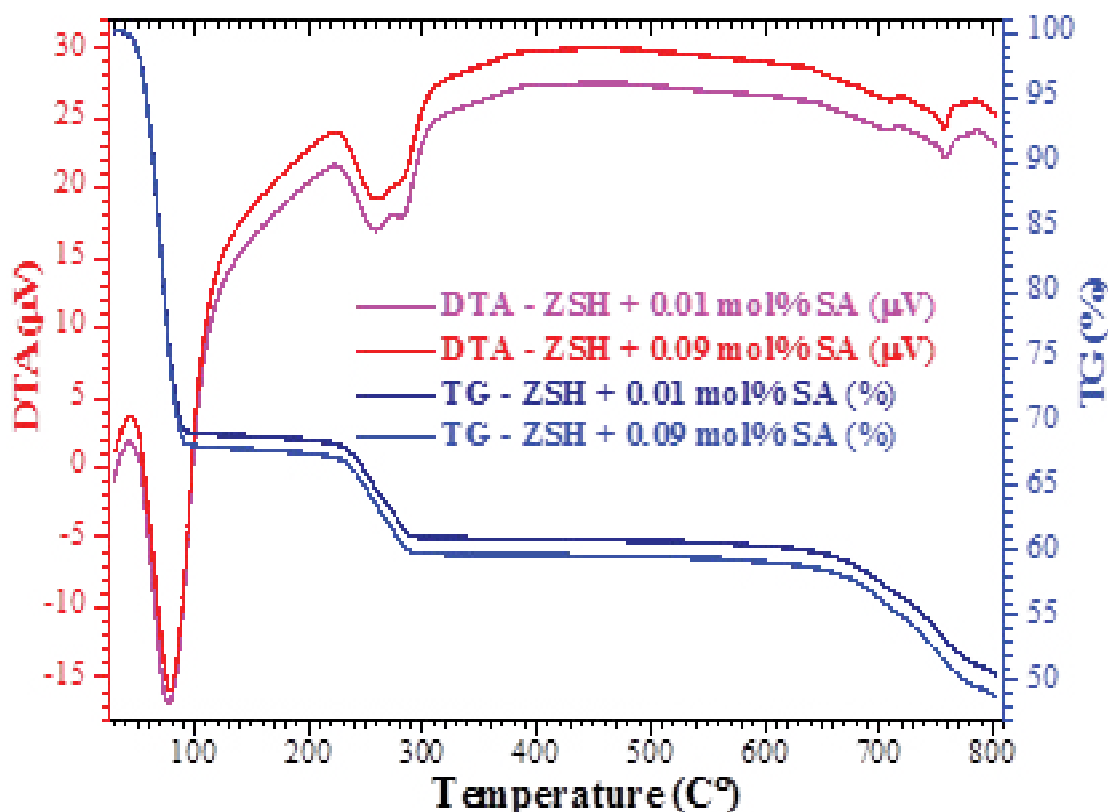


Figure 3: TG/DTA curves of 0.01 and 0.09 mol % SA doped ZSHSA

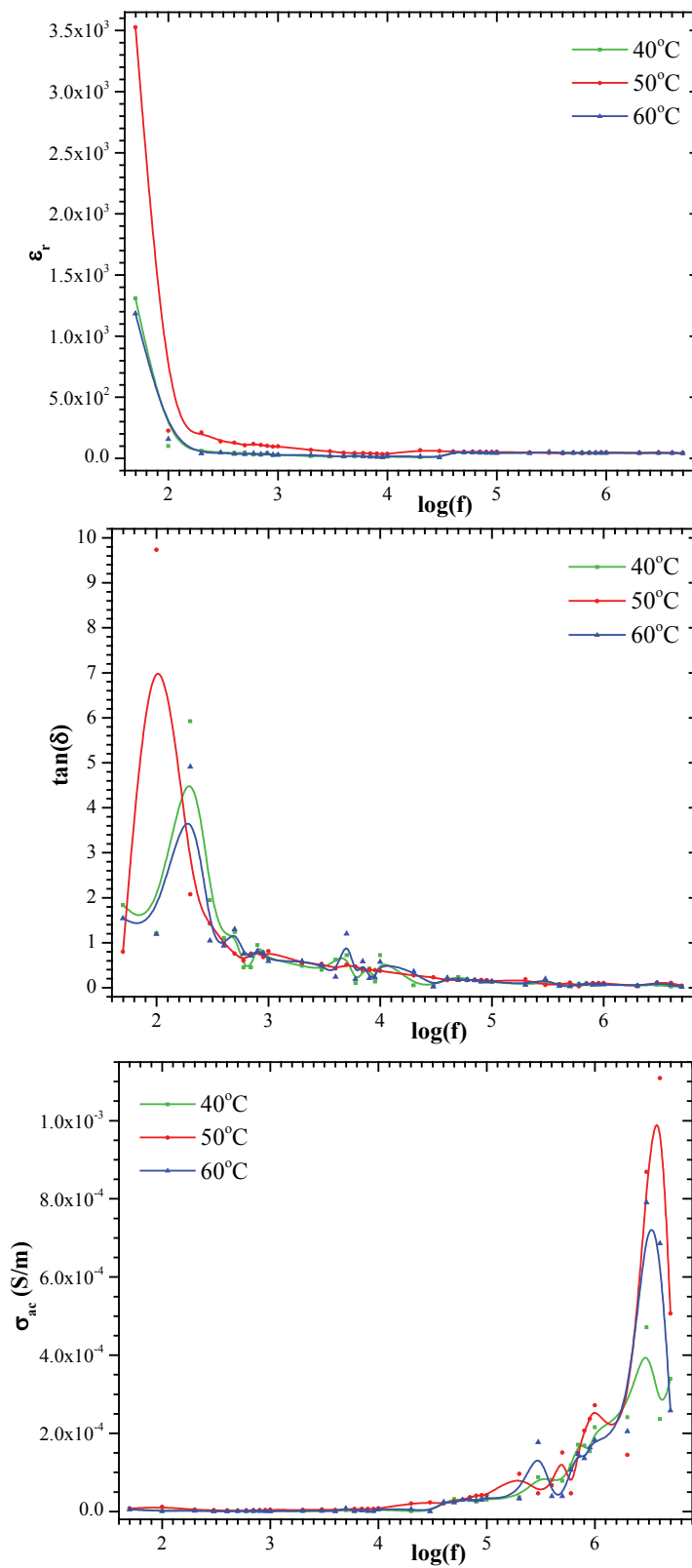


Figure 4: Variation of Dielectric constant, $\tan(\delta)$ and AC-conductivity with the frequency of the electric field of the ZSH+0.01 mol% SA crystals

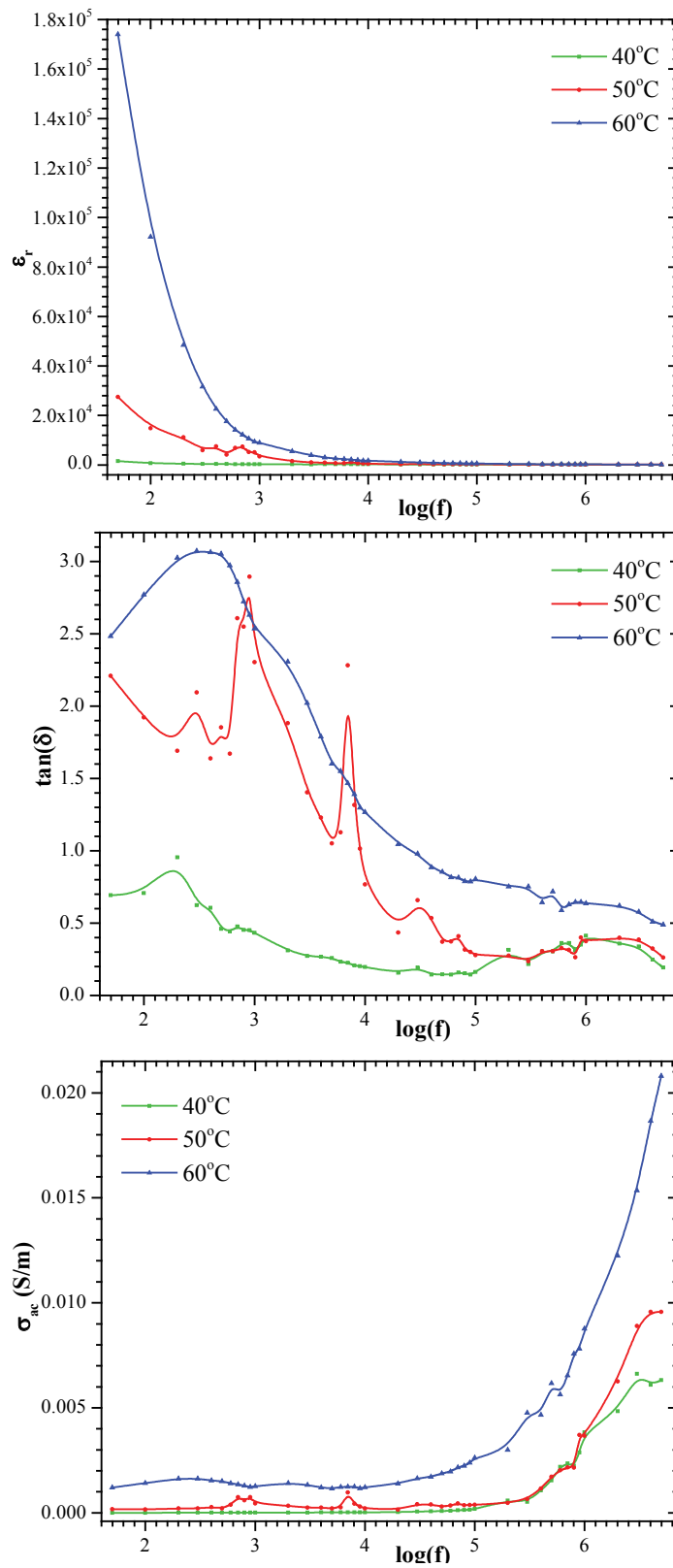


Figure 5: Variation of Dielectric constant, $\tan(\delta)$ and AC-conductivity with the frequency of the electric field of the ZSH+0.09 mol% SA crystals

Dielectric studies

Good quality ZSH and ZSHSA single crystals were selected for the dielectric measurements using LCR meter (Agilent 4284) from 50 Hz to 5 MHz for 40°C, 50°C and 60°C. The samples were cut and polished using paraffin oil and fine alumina powder to thin down them to the desired thickness dimensions and the parallel surfaces of contacts for testing were made conductive using silver paint to convert it to a capacitor with the crystal as the dielectric medium. As these crystals are non-conducting materials their dielectric properties are correlated with their electro-optic properties [26]. The plots (a), (b) and (c) of Figure 4 shows the frequency distribution of dielectric constant, dissipation factor $\tan(\delta)$ and ac conductivity, respectively for ZSH+0.01 mol% SA crystals and while Figure 5 is for ZSH+0.09 mol% SA crystals.

The dielectric constant (ϵ_r) of the crystals were evaluated using the relation [27,28],

$$\epsilon_r = \frac{Cd}{\epsilon_0 A}$$

where, C is the capacitance, d is the thickness of the sample between the plates, A is the area of overlap of the parallel silver painted crystal surfaces and ϵ_0 ($8.85 \times 10^{-12} \text{ C}^2 \text{ N}^{-1} \text{ m}^{-2}$) is the permittivity of free space. Both plots shown in Figures 4(a) and 5(a) show that, for all three temperatures ϵ_r decreases exponentially with the increase in frequency. The high value of the ϵ_r at low frequencies may be due to the presence of all four contributions of polarization such as, space charge, orientational, electronic and ionic polarization. The space charge polarization lowers the electrostatic binding strength near the grain boundary interfaces [28]. At lower frequencies, the electronic exchange of the number of ions in the crystals give local displacement of electrons in the direction of the applied field [29]. On the contrary, as the frequency increases, a point will be reached where the space charge cannot be sustained and comply with the variation of external field, hence polarization decreases, which gives rise to the diminishing of dielectric constant values. The low value of ϵ_r at high frequencies, may also be attributed to the significant fall in the above said four polarization contributions gradually [30]. This property of the crystals enhances their SHG efficiency, according to Miller rule.

Dielectric loss tangent or Dissipation Factor is calculated using the formula,

$$\tan(\delta) = \frac{1}{R_p \omega C_p}$$

where, C_p and R_p are parallel capacitive and resistive impedances, respectively [31]. From Figures 4(b) and 5(b) we observe that the frequency distribution of $\tan(\delta)$ also follows almost the same trend as the ϵ_r . The low value of $\tan(\delta)$ at higher frequencies suggests the crystals are of enhanced optical quality with lesser electrically active defects, which is an added advantage and requirement for the non-linear optical materials [28,32].

The AC conductivity σ_{ac} is calculated using the formula,

$$\sigma_{ac} = \epsilon_0 \epsilon_r \omega \tan \delta$$

The frequency distribution of σ_{ac} is shown in the Figures 4(c) and 5(c). In both, σ_{ac} increases with the increase in frequency. This dispersion trend in the σ_{ac} is the direct consequence of hopping of charge carriers around the lattice imperfections. The dispersion occurs when the carriers are not free to move through the sample [33].

As the doping concentration increases the ϵ_r too increases, as more free charge carriers are created by the dopant and may be due to incorporation of more impurities into the ZSH lattice [34]. And the increase in ϵ_r with temperature in Figure 5(a) is due to the thermally generated charge carriers and impurity dipoles [35], as the Curie point T_c is more than 60°C. This rapid increase may be due to the space charge polarization of these thermally generated carriers [36]. But the trend in Figure 4(a) is different, as it's T_c is between 40°C and 60°C, very close to 50°C. The increase in σ_{ac} with temperature, as seen in Figure 5(c), confirms that these crystals are insulating in nature, and this phenomenon is due to the transition of charge carriers from valence band to conduction band as the temperature of the crystal increases [37].

CONCLUSION

Zinc sulphate hepta hydrate single crystals without doping and with five different doping concentrations of 0.01, 0.03,

0.05, 0.07 and 0.09 mol% of succinic acid solutions were used to grow single crystals by slow evaporation technique. Through XRD data it is proved that all of these crystals belong to orthorhombic structure and non-centro-symmetric $P2_12_12_1$ space group. Fourier transform infrared spectra revealed the presence of all the functional groups of zinc sulphate hepta hydrate and of its dopant, succinic acid salt derivative too in the doped crystals. From the comparison of TG/DTA of the two doping concentrations of the ZSHSA crystals namely, 0.01 and 0.09 mol% SA, an increase in the melting point by 2°C with increase in concentration of SA dopant corroborates that the doping concentration comparatively enhances the thermal stability of the ZSHSA crystals. The ZSHSA crystals were found to decompose through two stages and it is confirmed that there are approximately 6½ to 7 water molecules of crystallization. The dielectric property studies at 40°C, 50°C and 60°C, indicate that the dielectric constant and dielectric loss decreases with the increase in frequency which is the normal behavior of nonlinear optical materials. The low dielectric constant and dielectric loss at high frequency region represent good optical quality of the grown crystals. AC conductivity of the grown crystals increases with temperature due to transition of charge carries from valence band to conduction band and the material is non-conducting in nature.

REFERENCES

1. Singh, N.H., *Appl Organomet Chem*, **1991**. 5(5): p. 377.
2. Min-Hua, J. and Fang, Q., *Adv Mater*, **1999**. 11(13): p. 1147.
3. Milton Boaz, B., Jerome Das., *J Cryst Growth*, **2005**. 279: p. 383-389.
4. Chandramohan, A., et al., *J Cryst Growth*, **2008**. 310: p. 5409-5415.
5. Vincent, C., et al., *J Cryst Growth*, **2004**. 267: p. 129-133.
6. Eazhilarasi, G., Nagalakshmi, R. and Krishnakumar, V., *Spectrochimica Acta Part A*, **2008**. 71: p. 502-507.
7. Shaokang, G., et al., *J Cryst Growth*, **2006**. 297: p. 361-365.
8. Rajesh, N.P., et al., *Materials Letters*, **2002**. 52: p. 326-328.
9. Hottenhuis, M.H.J. and Oudenampsen, A., *J Cryst Growth*, **1988**. 92(3-4): p. 513-529
10. Krishna Priya, R., Delphine, S.M. and Shobana, S., *Chem Asian J*, **2015**. 27(2): p. 582-586.
11. Thai, T.L.A., *Arch Appl Sci Res*, **2016**. 8 (11): p. 12-18.
12. John, C., R.A. Meyers (Ed.), **2000**. p. 10815-10837.
13. Ben, F., *Infrared Spectroscopy*, **1997**. 72.
14. Bhaskar, J. and Parthasarathy, G., *J Mod Phys*, **2010**. 1: p. 206-210.
15. Bernhard, S. (Edt), *Infrared and Raman Spectroscopy*, **1995**. 212.
16. Thomas, L. and Rebenstorf, B., *Acta Chem Scand*, **1991**. 45: p. 342-348.
17. John, T. (Edt.), *Reactions and Synthesis in Surfactant Systems*, **2001**. 649.
18. Joseph Bambert, B., *Introduction to Organic Spectroscopy*, **1987**. p. 174-177.
19. Foil Miller, A. and Charles, W.H., *Anal Chem*, **1952**. p. 1253-1294.
20. Vanitha, D., Bahadur, S.A. and Athimoolam, S., *Journal of Minerals and Materials Characterization and Engineering*, **2012**. 11: p. 1121-1125.
21. Masilamani, V., Shanthi, J. and Sheelarani, V., Hindawi Publishing Corporation, **2014**.
22. Sumithraj, P., Roy, S.D.D. and Shajan, X.S., *Chem Sci Trans*, **2014**. 3(1): p. 359-367.
23. Sweetly, A. and Chithambarathanu, T., *Int J Res Eng Technol*, **2014**. 3(5).
24. Radhika, S., et al., *Der Pharma Chemica*, **2012**. 4(5): p. 2014-2023.
25. Jianguo, P., et al., *J Cryst Growth*, **2007**. 308: p. 89-92.

26. Boomadevi, S. and Dhanasekaran, R., *J Cryst Growth*, **2004**. 261(1): p. 70-76.
27. Suresh, S., *Afr Rev Phys*, **2013**. 8(0006).
28. Suresh, S. and Anand, K., *Int J Chemtech Res*, **2013**. 5(1): p. 284-287.
29. Navamani, S.J., Sumithraj, P. and Narayanasamy, G., *International Journal of Scientific and Research Publications*, **2016**. 6(6).
30. Natarajan, N., Mahalakshmi, R. and Sagadevan, S., *Mater Res*, **2015**. 18(3): p. 581-587.
31. Aibeche, A., et al., *Proc Eng Technol*, **2013**. 4: p. 29-36
32. Radhika, S., et al., *Arch Phys Res*, **2013**. 4(1): p. 49-59.
33. Suresh, S., et al., *Arch Appl Sci Res*, **2010**. 2(4): p. 119-127.
34. Farhana, K. and Jiban, P., *Int J Optics*, **2012**.
35. Andavan, A.J.M., et al., *Indian J Sci Technol*, **2011**. 4(6): p. 688-691.
36. Shanthi, N.T., Selvarajan, P. and Mahadevan, C.K., *Indian J Sci Technol*, **2009**. 2(3): p. 49-52.
37. Indira, S., Ramesh, K. and Viruthagiri, G., *Indian J Sci Technol*, **2015**. 4(6); p. 363-366.